HHS Public Access

Author manuscript

Eur Polym J. Author manuscript; available in PMC 2021 March 15.

Published in final edited form as:

Eur Polym J. 2020 March 15; 127: . doi:10.1016/j.eurpolymj.2020.109598.

Electrosprayed poly(lactic-co-glycolic acid) particles as a promising drug delivery system for the novel JNK inhibitor IQ-1

Elina Kibler[a,1], **Anastasia Lavrinenko**[a,1], **Ilya Kolesnik**[a], **Ksenia Stankevich**[a,b], **Evgeny Bolbasov**[a,f], **Valeriya Kudryavtseva**[a,c], **Andrey Leonov**[a,d], **Igor Schepetkin**[b], **Andrei Khlebnikov**[a,e], **Mark T. Quinn**[b,*], **Sergei Tverdokhlebov**[a,*]

[a]National Research Tomsk Polytechnic University, Tomsk 634050, Russia

[b]Department of Microbiology and Immunology, Montana State University, Bozeman, MT 59717, USA

[c]School of Engineering and Materials Science, Queen Mary University of London, London E1 4NS, United Kingdom

[d]Institute of High Current Electronics, Siberian Branch, Russian Academy of Sciences, Tomsk 634055, Russia

[e]Faculty of Chemistry, National Research Tomsk State University, Tomsk 634050, Russia

[f]Microwave Photonics Lab, Institute of Atmospheric Optics V.E. Zuev SB RAS, Tomsk 634055, Russia

Abstract

Mitogen-activated protein kinases (MAPKs), including c-Jun N-terminal kinase (JNK), play important role in the regulation of pro-inflammatory cytokine secretion and signaling cascades. Therefore, JNKs are key targets for the treatment of cytokine/JNK-driven diseases. Herein, we developed electrospray poly(lactic-co-glycolic acid) (PLGA) microparticles doped with novel JNK inhibitor 11*H*-indeno[1,2-*b*]quinoxalin-11-one oxime (IQ-1). Optimized electrospray parameters allowed us to produce IQ-1-doped microparticles with round shape, smooth and non-porous surface, and mean diameter of 0.9–1.3 μm. We have shown that IQ-1 was well integrated into the polymer matrix and had a prolonged release in two steps via non-Fickian release. The fabricated particles doped with IQ-1 exhibited anti-inflammatory effects, as indicated by inhibited neutrophil activation and cytokine secretion by human monocytic MonoMac-6 cells. Overall, our study

*Corresponding authors at: The Weinberg Research Center, National Research Tomsk Polytechnic University, Tomsk 634050, Russia (S. Tverdokhlebov)., mquinn@montana.edu (M.T. Quinn), tverd@tpu.ru (S. Tverdokhlebov).

[1]These authors have contributed equally to the study.

CRediT authorship contribution statement

Elina Kibler: Investigation, Writing - original draft. **Anastasia Lavrinenko:** Investigation, Writing - original draft, Writing - review & editing. **Ilya Kolesnik:** Investigation. **Ksenia Stankevich:** Investigation, Writing - review & editing, Funding acquisition. **Evgeny Bolbasov:** Investigation, Writing - original draft, Writing - review & editing, Funding acquisition. **Valeriya Kudryavtseva:** Investigation. **Andrey Leonov:** Investigation. **Igor Schepetkin:** Validation, Funding acquisition, Resources. **Andrei Khlebnikov:** Validation, Funding acquisition, Resources. **Mark T. Quinn:** Conceptualization, Funding acquisition, Resources. **Sergei Tverdokhlebov:** Conceptualization, Project administration, Resources, Supervision.

Declaration of Competing Interest

The authors declare that they have no known competing financial interests or personal relationships that could have appeared to influence the work reported in this paper.

demonstrates that PLGA microparticles doped with a novel JNK inhibitor (IQ-1) could be a promising delivery system for treatment of JNK-mediated diseases.

Keywords

Electrospray; Drug delivery; Poly(lactic-co-glycolic acid); c-Jun N-terminal kinase inhibitor

1. Introduction

Mitogen-activated protein kinases (MAPKs), including p38 MAPK, extracellular signal-regulated kinase, and c-Jun N-terminal kinase (JNK) have become attractive therapeutic targets, since JNKs are involved in apoptosis, necrosis, inflammation [1,2], and ischemia/reperfusion injury [3]. Indeed, JNKs play important roles in the pathogenesis of numerous diseases including insulin resistance [4], cancer [5], Alzheimer's and Parkinson's diseases [6], and rheumatoid arthritis (RA) [7]. In particular, JNKs regulate pro-inflammatory cytokine secretion and signaling cascades that lead to joint inflammation and destruction, heart failure, ischemia-induced myocardial dysfunction, development of insulin resistance, and airway smooth muscle dysfunction [8,9]. Therefore, JNK inhibition has a significant therapeutic potential for treatment of cytokine/JNK-driven diseases. For example, it has been shown in a mouse antigen-induced arthritis model that inhibition of JNK-1 reduces infiltration of inflammatory cells and joint damage [7].

Recently, we found that the JNK inhibitor IQ-1S (11*H*-indeno[1,2-*b*] quinoxalin-11-one oxime sodium salt), shown on Fig. 1, significantly diminished the clinical severity of CIA and inhibited cartilage and bone destruction in a mouse collagen-induced arthritis (CIA) model, demonstrating its therapeutic potential in the treatment of RA [10]. Additionally, IQ-1S was shown to have neuroprotective properties in mouse models of cerebral reperfusion [11] and in a model of global cerebral ischemia in rats [12]. The corresponding oxime of IQ-1S, IQ-1 (11*H*-indeno[1,2-*b*]quinoxalin-11-one oxime) was found to have pronounced anti-inflammatory effects in human monocytic cell lines [13,14]. IQ-1 can easily be synthesized and purified and has high selectivity against JNKs (K_d for JNK1-3 are 0.24, 0.36, and 0.10 μM, respectively). On the other hand, its poor water solubility may negatively affect further clinical application.

Solubility issues can be addressed by encapsulation of IQ-1 into biodegradable polymer nano- or micro-carriers that can be further delivered into inflammatory sites to release the compound in a controlled manner. Various techniques for manufacturing drug-doped particles are reported to date, including emulsion and spray drying methods [15–19]. However, in addition to being lengthy procedures, these methods often suffer from low drug encapsulation efficiency [19,20]. The encapsulation of IQ-1 is also complicated by its poor solubility in most organic solvents and its tendency to crystallize. To address these issues, a promising approach to manufacture the desired drug delivery system is electrospray (ES). Over the past decade, ES has proven itself as a versatile method for the synthesis of polymer particles with tight control over particles size, high encapsulation efficiency, minimal agglomeration, and the desired release profile [21–23]. One of the most widely used

polymers in drug delivery is poly(lactic-co-glycolic) acid (PLGA) due to its biocompatibility, injectability, ease of formulation, and the potential for controlled degradation rate [24–26]. We discovered that a sufficient amount of IQ-1 could be dissolved together with PLGA in dimethylformamide (DMF). Therefore, ES is a feasible method for creating PLGA/IQ-1 carriers.

Herein, we aimed to design and produce PLGA particles doped with IQ-1 using ES and to study their anti-inflammatory effects *in vitro*.

2. Materials and methods

2.1. Fabrication of polymer microparticles

Poly(lactic-co-glycolic acid)-based microparticles were manufactured by ES using NANON-NF 101 (MECC Co., Japan) equipment with the following technological parameters: 27G syringe tip, distance between the collector and the needle of 150 ± 5 mm, flow rate of the polymer solution of 0.50 ± 0.05 mL/h, and voltage of 27 ± 3 kV. Unloaded PLGA particles were produced from 10 wt% DMF solution of poly(lactic-co-glycolic acid) (PLGA, lactide:glycolide = 50:50; M_w = 45000 g/mol, Sigma-Aldrich). 11*H*-indeno[1,2-*b*]quinoxalin-11-one oxime (IQ-1) was synthesized, as previously described [13,14]. To obtain IQ-1-loaded microparticles, DMF solutions containing 10 wt% of PLGA and 5, 10, or 20% of IQ-1 were prepared. One wt.% water solution of polyvinyl alcohol (PVA, M_w = 89000–98000 g/mol, Sigma-Aldrich) was used as particle stabilizer. The resulting microparticles were harvested and cleaned by centrifuging and washing 3 times with distilled water. Finally, particles were dried until constant weight and stored under ambient temperature. Theoretical drug loading of IQ-1 was determined as follows:

$$\text{Theoretical drug loading} = \frac{\text{Weight of } \mathbf{IQ}1}{\text{Weight of PLGA}} \cdot 100\,\% \tag{1}$$

2.2. Scanning electron microscopy

Investigation of the morphology of formed particles was conducted by scanning electron microscopy (SEM) using a Vega 3 SBH electron microscope (TESCAN, Czech Republic). The surface of PLGA microparticles was coated with a thin gold layer using a magnetron sputtering system SC7640 (Quorum Technologies Ltd, UK). The large (d_{max}) and small (d_{min}) particle diameters were determined using ImageJ software (National Institutes of Health, USA) for 10 digital images with × 10000 magnification. The aspect ratio (AR) was calculated in accordance with ASTM F1877–16 [27] recommendations using the equation (2):

$$AR = \frac{d_{\max}}{d_{\min}} \tag{2}$$

Average diameter of the PLGA particles was calculated from ≥ 300 measurements.

2.3. Encapsulation efficiency

To measure the amount of incorporated IQ-1, 3.5 mg of microparticles were immersed into 4 mL of dimethyl sulfoxide (DMSO) and kept for 24 h. The concentration of released IQ-1 was evaluated using a UV-Visible spectrophotometer (Thermo Scientific Evolution 600, England) by monitoring the absorbance at wavelength of 288 nm. Non-loaded PLGA particles were used as reference. The calibration curve for the compound was previously traced using the absorption maximum from its spectrum at 288 nm. The practical drug loading of IQ-1 and encapsulated efficiency (EE) were calculated as follows:

$$\text{Practical drug loading} = \frac{\text{Amount of released } \mathbf{IQ}1}{\text{Amount of PLGA}} \cdot 100\,\% \tag{3}$$

$$\text{EE} = \frac{\text{Amount of released } \mathbf{IQ}1}{\text{Amount of loaded } \mathbf{IQ}1} \cdot 100\,\% \tag{4}$$

where the amount of PLGA and loaded IQ-1 were calculated considering the weight of the samples (3.5 mg) and the theoretical drug loading of IQ-1 (5, 10, or 20%). Three independent experiments were performed, with each experiment containing 3 replicates.

2.4. IQ-1 release kinetics

Fifteen mg of dried PLGA particles were resuspended in 7 mL of phosphate buffered saline (PBS, pH 7.4) and maintained at 37 °C for 90 days. The amount of compound released into the medium was determined using a UV–Visible spectrophotometer (Thermo Scientific Evolution 600, England) at appropriate time intervals. At each time, the experimental solution was centrifuged at 5000 rpm for 5 min, and an aliquot of 2 mL was collected from the supernatant. An equal volume of fresh PBS was added back to the experimental solution after each removal to maintain a constant amount of solvent. A standard calibration curve was previously traced using the absorption maximum from the IQ-1 spectrum at 288 nm. Non-loaded PLGA particles were used as reference.

The percentage of the released IQ-1 was calculated as follows:

$$\text{Release percentage} = \frac{\text{Amount of released } \mathbf{IQ}1}{\text{EE} \cdot \text{Amount of loaded } \mathbf{IQ}1} \cdot 100\,\% \tag{5}$$

where the amount of loaded IQ-1 was calculated considering the weight of the samples (15 mg) and theoretical drug loading of IQ-1 (5, 10 or 20%).

To evaluate the IQ-1 release mechanism, several kinetic models were applied, i.e. zero-order kinetics, first-order kinetics, Higuchi model, and Ritger–Peppas model. The working kinetic models are described by the following equations [28]:

• Zero-order kinetics:

$$f = k_0 t \tag{6}$$

• First-order kinetics:

$$f = 1 - e^{-k_1 t} \quad (7)$$

• Higuchi model:

$$f = k_H t^{0.5} \quad (8)$$

• Ritger–Peppas model:

$$f = k_p \cdot t^n \quad (9)$$

where f is the percentage of cumulative compound release at time (t); k_0, k_1, k_H, and k_p are the constants of the respective kinetic models; and n is the exponent from the Ritger–Peppas model.

According to the kinetic models, the release data were plotted as cumulative percentage of drug released vs. time (zero-order kinetics); natural log cumulative percentage of drug remaining vs. time (first-order kinetics); cumulative percentage drug released vs. square root of time (Higuchi model); and natural log cumulative percentage drug released vs. natural log time (Ritger-Peppas model) [29]. The presented correlation coefficient (R^2) values were calculated from the linear regression of the aforementioned plots. Three independent experiments were performed, with each experiment containing 3 replicates.

2.5. Thermal analysis

Thermal analysis was carried out using a simultaneous differential scanning calorimetry/thermogravimetric analysis (DSC/TGA) instrument SDT-Q600 (TA Instruments, Delaware, USA). The DSC/TGA runs were made in dynamic air atmosphere (100 mL/min) using aluminum pans, a heating rate of 10 °C/min, and a temperature range of 25–450 °C. A typical sample weight was 10 mg. Three independent experiments were performed, with each experiment containing 3 replicates.

2.6. X-ray diffraction

Crystallinity of the IQ-1 powder and polymer particles was investigated by X-ray diffraction analysis (XRD) using a Shimadzu X-ray diffractometer 6000 (Shimadzu, Japan). Measurements were conducted in the range of angles 2θ 0 – 90°, shooting speed of 2° per min, and step of 0.02°. A standard Cu X-ray tube was used for the measurements. Three independent experiments were performed, with each experiment containing 2 replicates.

2.7. Biological studies

To conduct biological studies, powdered particles doped with different amount of IQ-1 were resuspended in PBS at a concentration of 1 mg/mL, aliquoted, and stored at −20 °C.

2.8. Isolation of human neutrophils

Neutrophils were isolated from human blood using sequential dextran sedimentation, differential density sedimentation in a Histopaque 1077 gradient and hypotonic lysis of red

blood cells, as described previously [30]. Blood was collected from the healthy donors according to a protocol approved by the Institutional Review Board at Montana State University. Cell preparations were routinely > 95% pure, as determined by light microscopy, and > 98% viable, as determined by trypan blue exclusion. Purified neutrophils were resuspended at 10^7 cells/mL in HBSS without Ca^{2+} and Mg^{2+} ($HBSS^-$).

2.9. Reactive oxygen species (ROS) detection

The level of ROS production was monitored using a cytochrome C reduction assay. Prior to the cell addition, particles were aliquoted from the stock suspension into the wells of a 96-well plate over the dilution range of 0–500 μg/mL, and cytochrome C (from bovine heart, Sigma-Aldrich) was added to each well at a concentration of 1 mg/mL. Freshly isolated human neutrophils were resuspended at 10^7 cells/mL in HBSS containing Ca^{2+} and Mg^{2+} ($HBSS^+$) and aliquoted at 5×10^5 cells/well. Total volume of the media in each well was 200 μL. Neutrophils incubated without particles were used as a negative control. Neutrophils incubated without particles and stimulated with 100 nM phorbol 12-myristate 13-acetate (PMA) were used as positive control. The absorbance at 550 nm indicating cytochrome *C* reduction was monitored over 2 h with a 1-min interval at 37 °C using a SpectraMax® Plus 384 microplate reader. The amount of ROS production was calculated from the absorbance reading using the molecular extinction coefficient for cytochrome C (28000 $M^{-1}cm^{-1}$). The data are presented as mean ± SD of duplicate samples. A representative experiment from three independent experiments is shown.

2.10. MonoMac-6 cell culture

Human monocyte-macrophage MonoMac-6 cells (Deutsche Sammlung von Mikroorganismen und Zellkulturen GmbH, Braunschweig, Germany) were grown in RPMI 1640 medium supplemented with 10% (v/v) fetal bovine serum, 10 mg/mL bovine insulin, 100 mg/mL streptomycin, and 100 U/mL penicillin. Cells were cultured at 37 °C in a humidified atmosphere containing 5% CO_2.

2.11. Cell viability assay

Cytotoxicity of the particles towards MonoMac-6 cells was analyzed with a CellTiter-Glo Luminescent Cell Viability Assay Kit from Promega (Madison, WI, USA), according to the manufacturer's instructions. Prior to cell addition, particles were aliquoted from the stock suspension into the wells of a 96-well plate over the dilution range of 0–500 μg/mL. MonoMac-6 cells were aliquoted at 1.5×10^5 cells/well and cultured for 24 h. MonoMac-6 cells incubated without particles were used as a control. After 24 h, the cells were allowed to equilibrate to room temperature for 30 min, substrate was added, and the samples were analyzed with a Fluoroscan Ascent FL (Thermo Fisher Scientific, Waltham, MA, USA). The viability was calculated in percentage relative to control. The data is presented as mean ± SD of 2 repeats from one experiment. A representative experiment from three independent experiments is shown.

2.12. Analysis of cytokine secretion

The effect of particles on interleukin 6 (IL-6) production by MonoMac-6 cells was evaluated using a human IL-6 ELISA kit (BD Biosciences, San Jose, CA, USA). Prior to cell addition, particles were aliquoted from the stock suspension into the wells of a 96-well plate over the dilution range of 0–500 μg/mL. MonoMac-6 cells were aliquoted at 1.5×10^5 cells/well and cultured for 24 h. Alternatively, MonoMac-6 cells were pre-incubated with particles for 30 min, followed by the addition of 200 ng/mL lipopolysaccharide (LPS) for 24 h. MonoMac-6 cells incubated without particles were used as a control. IL-6 concentration in pg/mL was compared was with positive control samples (LPS) and negative control samples (MonoMac-6 cells without LPS). The data are presented as mean ± SD of 2 repeats from one experiment. A representative experiment from three independent experiments is shown.

2.13. Statistical analysis

All data were analyzed using one-way ANOVA with Tukey's correction in GraphPad Prism 8 software. Differences were considered statistically significant at $p \leq 0.05$.

3. Results and discussion

Polymeric particles represent promising drug delivery system due to their ability to circulate inside the body and reach local target sites [31]. Polymer selection is an important part of the particle design, as polymer properties influence toxicity, pharmacokinetics, and biocompatibility of the drug delivery system [32]. For example, PLGA has attracted considerable attention in the field of drug delivery due to its biocompatibility, injectability, manufacturability, and controlled degradation rate [24–26]. Herein, we manufactured and evaluated PLGA particles doped with the JNK inhibitor IQ-1 as a promising drug delivery system that could be developed for the treatment of cytokine/JNK-driven diseases, such as RA or cerebral ischemia.

Given the poor solubility of IQ-1 in most organic solvents and water, the first objective was to determine the optimal technological parameters for PLGA particle production by electrospray. Physico-chemical and technological parameters, such as liquid flow rate, electrical conductivity, viscosity of the solvent, voltage, distance to collector, needle gauge, polymer and drug concentration, can influence particle size and distribution [22,33,34].

The parameters of particles doped with different concentrations of IQ-1 are presented in Table 1. The abbreviations used in Table 1 are used throughout the manuscript in reference to the different sample groups. Representative SEM images and diameter distribution of PLGA/IQ-1 particles are shown in Fig. 2. The majority of the particles had a round shape, which is supported by aspect ratio values close to 1 (Table 1). The surface of the particles was smooth without visible pores, which could be explained by the influence of solvent evaporation rate. It is known, that the use of solvents with high boiling points allows one to decrease evaporation rate and obtain a dense surface with low porosity [35].

One of the key factors in design of particles is particle size, as this parameter can affect encapsulation efficiency, product injectability, drug release rate, and side-effect profiles [36,37]. The mean diameters of the microparticles shown in Table 1 demonstrate that the rise

of IQ-1 concentration reduced the mean particle size. This could be caused by the influence of the spinning solution parameters. Apparently, the addition of IQ-1 to the spinning solution resulted in a rise of electrical conductivity and decrease of solution viscosity. These changes led to a decrease in the particle diameters [38–40].

High encapsulation efficiency of the drug is preferable for its optimal usage since it allows reduction of the concentration of particles required to achieve a particular effective dose. The practical drug loading and encapsulation efficiency are presented in Table 1 as mean ± SD based on three independent measurements. It is evident that the encapsulation efficiency increased with the increase in theoretical drug loading, which could be caused by compound saturation effects of the outer aqueous phase during particle formation [41].

The degree of crystallinity of compound and polymer, compound distribution, and polymer-compound interaction are important factors influencing release pattern. Such characteristics can be assessed with XRD and DSC/TGA measurements [22]. XRD measurements were employed to examine IQ-1 distribution in the polymer matrix of the microparticles [42,43]. Several well-defined peaks in the XRD pattern of IQ-1 powder (Fig. 3) indicated that IQ-1 powder is highly crystalline [43,44], whereas the PLGA particles are amorphous. The process of fast evaporation of the organic solvent during electrospraying and subsequent particle formation prevents crystallization of the polymer due to reduced time for polymer reorganization [45]. We found that the X-ray diffraction patterns of PLGA/IQ-1 micro particles were similar to pure PLGA micro particles. There were no significant changes observed in X-ray diffraction pattern of PLGA_5 particles. This might be due to the presence of extremely small IQ-1 crystals, which could not be detected by XRD or compound being dissolved in the polymeric matrix [41,43]. However, a small reflex in the 2θ range of 10.7–12.8° and a small reflex in the 2θ range of 10.7–12.8° and 23.8–24.6° related to crystalline IQ-1 could be observed in the X-ray diffraction pattern of particles PLGA_10 and PLGA_20, respectively.

Complementary to XRD, the DSC/TGA data allow elucidating the physical state of IQ-1 in the PLGA matrix, as well as the interaction and thermal transitions of the compounds [22,43,46,47].

DSC and TGA thermograms of pure IQ-1 powder and PLGA microparticles are presented at Fig. 4A and Fig. 4B, respectively. The DSC thermogram of pure IQ-1 showed a slight endothermic peak at 43 °C, occurring apparently due to crystallization and desolvation. Two peaks observed at 275 °C and 281 °C could be attributed to IQ-1 melting followed by thermal decomposition [48] (Fig. 4A). The presence of a melting peak indicates a crystalline state of IQ-1 in powder. TGA curves of pure IQ-1 showed the weight loss started at about 254 °C and achieved 26.5% at 450 °C (Fig. 4B).

The DSC curve of PLGA_0 microparticles showed an endothermic peak at 52 °C corresponding to PLGA glass transition temperature [49] (Fig. 4A). No peak attributed to the PLGA melting was observed, indicating the amorphous state of the polymer. This finding is coherent with the XRD results (Fig. 3). Two peaks at 359 °C and 384 °C can be attributed to PLGA thermal degradation that is supported by the weight loss of 90.2% in the

range of 296–450 °C. Below the indicated temperature range PLGA_0 microparticles were thermally stable (Fig. 4B).

For the microparticles doped with IQ-1, the correlation between the depression of degradation temperature or weight loss and the rise of encapsulated IQ-1 amount from PLGA_0 to PLGA_20 could be observed. Thus, according to the TGA results, an increase of the compound loading from 0% to 20% lead to a decrease in the weight loss from about 90% to 80% (Fig. 4B). Thermal degradation temperature of PLGA was lowered from 384 °C to 372, 369 and 361 °C for PLGA_5, PLGA_10 and PLGA_20 samples, respectively (Fig. 4A). The depression of thermal degradation temperature could be caused by both IQ-1 acting as an additive and the decrease of a particle diameter (Table 1). It was shown that microparticles with a lower diameter tend to degrade easier due to a larger area [50]. The melting peaks of IQ-1 were not observed in the thermograms of IQ-1-doped microparticles (Fig. 4A). It can be explained by either an amorphous state of the compound-polymer composite or by the integration of IQ-1 into the polymer matrix. The latter is supported by the absence of PLGA glass transition peak in the thermograms of IQ-1 -doped particles. Additionally, it is known that better encapsulated systems have an obscure melting peak of the drug [22,51]. The appearance of exothermic peaks in the range of 220–250 °C for PLGA_10 and PLGA_20 (Fig. 4A) exhibited the complicated interactions between IQ-1 and PLGA matrix under high temperatures. The explanation of such effect requires further studies.

Fig. 5 shows the IQ-1 release profile for the PLGA particles over 90 days. After 90 days, the cumulative compound release approached 100%, 38%, 15% for PLGA_5, PLGA_10, and PLGA_20, respectively. As IQ-1 concentration increased, the amount of released compound was dramatically reduced. This can be explained by IQ-1 hydrophobicity [13], as hydrophobic drugs loaded into particles are known to release slower at higher drug concentrations [52].

Drug release from polymer particles occurs by several mechanisms, including desorption of the surface-bound/adsorbed drug, diffusion through the polymer, and polymer surface erosion [53–55]. The release profile of IQ-1 from PLGA particles can be described as a biphasic process. All samples showed a burst release within the first hour (Fig. 5, Inset), followed by an approximately first-order sustained release.

The rapid initial release was mainly attributed to compound weakly bound or adsorbed to the large surface of the particles [53]. The second phase (steady release) is related to diffusion and hydrolysis [56]. Due to the fastest degradation rate for PLGA (50:50) of 1–2 months in aqueous conditions [25,26,56], the drug release from PLGA micro- and nano-systems should have a third phase caused by bulk erosion, which results in rapid release in a later stage [56]. However, rapid release in the later stage was not observed, apparently, due to the poor compound solubility in water. Hence, the results indicated that IQ-1 release from PLGA particles was defined by the diffusion stage and showed mainly a prolonged effect.

Commonly used kinetic models (zero-order kinetics, first-order kinetics, and the Higuchi and Ritger–Peppas models) were applied to describe the dependence of release in function

of time. The Ritger–Peppas model was applied to determine the IQ-1 release mechanism. The calculated release exponent (n) for PLGA_5, PLGA_10, and PLGA_20 was > 0.43 (Table 2), indicating a non-Fickian release mechanism that was controlled by diffusion and swelling [57]. Among the applied kinetic models (zero-order, first-order, Higuchi and Ritger–-Peppas models) Higuchi model best described the release data for PLGA_5 as this model showed the highest R^2 value compared to the zero-order and first-order models (Table 2). In the case of PLGA_10 and PLGA_20 first-order kinetic model best described the dependence of release in function of time. So, in the case of low drug loading the release was mainly controlled by the IQ-1 diffusion process [28], but with the increase of drug loading and appearance of crystalline IQ-1 in the PLGA matrix the release rate was influenced by the adsorption and elimination of drug [28].

We next evaluated the biological properties of our particles fabricated using the parameters described above. Neutrophils are among the key cells involved in the innate immune response [58] and play an important role in pathogenesis of RA, as they secrete cytokines and chemokines that mediate inflammation and cell migration, produce reactive oxygen species (ROS) and release neutrophil extracellular traps [59,60]. In a mouse arthritis model, it was shown that neutrophil depletion inhibited arthritis development and reduced inflammation and bone damage [61]. Therefore, in order to study anti-inflammatory effects of the manufactured particles doped with IQ-1, we isolated human neutrophils and cultured them in the presence of polymer carriers. ROS production was measured to assess neutrophil activation.

The results showed that PLGA microparticles activated neutrophil ROS production in a dose-dependent manner (Fig. 6A). Previously, it was found that the uptake of PLGA particles by *ex vivo* neutrophils is size-dependent: microparticles (> 1 μm) are taken up better than nanoparticles [62]. Additionally, it has been shown that there is a correlation between particles internalization and ROS production by neutrophils [63]. Therefore, given the size of the manufactured particles, we can assume that at high concentrations, more particles are rapidly internalized, leading to neutrophil activation and elevated ROS production. However, regardless of the concentration added, neutrophil activation by PLGA particles was still much less than that induced by PMA (Fig. 6B).

ROS production in response to PLGA particles containing IQ-1 was significantly decreased compared to bare PLGA (Fig. 6), and ROS production decreased with increasing concentrations of IQ-1 embedded into the particles. Indeed, PLGA particles containing the highest amount of IQ-1 (PLGA_20) completely inhibited ROS over all particles concentrations evaluated (Fig. 6A). The observed effects are consistent with our previous studies, where we found that IQ-1 inhibited ROS production by human neutrophils stimulated with polymer biomaterials [64].

Another key cells that play a pivotal role in cytokine/JNK-driven diseases development are macrophages/monocytes [65,66]. They have been shown to infiltrate synovial membranes and upon activation secrete pro-inflammatory cytokines, chemokines, and metalloproteinases, which contribute to inflammation and joint destruction [67]. To study the effect of the manufactured particles on macrophage/monocyte pro-inflammatory

responses, we evaluated the influence of PLGA/IQ-1 on LPS-induced IL-6 secretion by human monocytic MonoMac-6 cells.

As shown in Fig. 7, PLGA microparticles induced elevated IL-6 secretion by non-stimulated MonoMac-6 cells in a concentration-dependent manner (Fig. 7A), whereas PLGA microparticles doped with IQ-1 did not stimulate IL-6 production over all concentrations tested (Fig. 7A). PLGA microparticles did not elicit elevated IL-6 secretion by LPS-stimulated MonoMac-6 cells, while PLGA microparticles containing IQ-1 inhibited IL-6 production (Fig. 7B). This effect was concentration dependent, as higher concentrations of encapsulated IQ-1 led to lower levels of IL-6 secretion. Similarly, as more particles were added, less IL-6 production was observed (Fig. 7B). These results are supported by our previous studies showing that IQ-1 suppressed LPS-induced IL-6 secretion by MonoMac-6 cells with an IC_{50} value of 3.8 ± 0.8 μM [13].

To confirm that the observed results were not due to the particle toxicity, cytotoxicity of the PLGA_0 and PLGA/IQ-1 particles towards MonoMac-6 was assessed (Fig. 8). Notably, the particles did not affect cell viability, indicating that they were not cytotoxic during the assay incubation period.

Therefore, PLGA particles doped with IQ-1 (20%) inhibited neutrophil activation and pro-inflammatory cytokine secretion by human monocytic MonoMac-6 cells and exhibited overall anti-inflammatory potential.

4. Conclusions

Herein, we fabricated PLGA microparticles doped with novel JNK inhibitor IQ-1 as a promising drug delivery system for development in cytokine/JNK-driven disease treatment. Optimized electrospray parameters allowed us to produce IQ-1-doped microparticles with a round shape, a smooth, non-porous surface, and a mean diameter in the range of 0.9–1.3 μm. Our results indicate that IQ-1 was well integrated into the PLGA matrix and tended toward a prolonged release through non-Fickian mechanism controlled by diffusion and swelling. Notably, the fabricated PLGA microparticles doped with IQ-1 inhibited neutrophil activation and pro-inflammatory cytokine secretion by human monocytic MonoMac-6 cells, which is important since phagocytes play a pivotal role in inflammation development. Notably, the investigated particles did not affect cell viability and were not cytotoxic during the assay incubation period. Future research is required in order to investigate the *in vivo* potential of these PLGA microparticles doped with IQ-1.

Acknowledgments

This research was supported in part by United States Department of State Fulbright Visiting Student Researcher Program (Grant ID PS00261116); National Institutes of Health IDeA Program Grants GM110732, GM115371, and GM103474; USDA National Institute of Food and Agriculture Hatch project 1009546; the Montana State University Agricultural Experiment Station; Tomsk Polytechnic University Competitiveness Enhancement Program and Russian State Project “Science” (WSWW-2020-0011). Compound synthesis and drug release studies were supported by the Russian Science Foundation grant No. 17-15-01111. Investigation of the morphology of formed particles was supported by the Russian Academy of Sciences (Fundamental Research Project no. AAAA-A19-119110690036-9). The authors acknowledge the Shared Knowledge Center “Physical and Chemical Analysis Methods” of Tomsk Polytechnic University for providing analytical equipment. We would like to thank Professor Gleb Sukhorukov for suggestions and his invaluable expertise in drug delivery systems.

References

[1]. Bogoyevitch MA, Ngoei KRW, Zhao TT, Yeap YYC, Ng DCH, c-Jun N-terminal kinase (JNK) signaling: Recent advances and challenges, Biochim. Biophys. Acta - Proteins Proteomics. 2010 (1804) 463–475, 10.1016/j.bbapap.2009.11.002.

[2]. Ip YT, Davis RJ, Signal transduction by the c-Jun N-terminal kinase (JNK) — from inflammation to development, Curr. Opin. Cell Biol. 10 (1998) 205–219, 10.1016/S0955-0674(98)80143-9. [PubMed: 9561845]

[3]. Shvedova M, Anfinogenova Y, Atochina-Vasserman EN, Schepetkin IA, Atochin DN, c-Jun N-Terminal Kinases (JNKs) in Myocardial and Cerebral Ischemia/Reperfusion Injury, Front. Pharmacol. 9 (2018), 10.3389/fphar.2018.00715.

[4]. Solinas G, Becattini B, JNK at the crossroad of obesity, insulin resistance, and cell stress response, Mol. Metab. 6 (2017) 174–184, 10.1016/j.molmet.2016.12.001. [PubMed: 28180059]

[5]. Koch P, Gehringer M, Laufer SA, Inhibitors of c-Jun N-terminal kinases: an update, J. Med. Chem. 58 (2015) 72–95, 10.1021/jm501212r. [PubMed: 25415535]

[6]. Zhang G-Y, Zhang Q-G, Agents targeting c-Jun N-terminal kinase pathway as potential neuroprotectants, Expert Opin. Investig. Drugs. 14 (2005) 1373–1383, 10.1517/13543784.14.ll.1373.

[7]. Guma M, Ronacher LM, Firestein GS, Karin M, Corr M, JNK-1 deficiency limits macrophage-mediated antigen-induced arthritis, Arthritis Rheum. 63 (2011) 1603–1612, 10.1002/art.30271. [PubMed: 21305529]

[8]. Thalhamer T, McGrath MA, Harnett MM, MAPKs and their relevance to arthritis and inflammation, Rheumatology 47 (2007) 409–414, 10.1093/rheumatology/kem297.

[9]. Cuenda A, Rousseau S, p38 MAP-Kinases pathway regulation, function and role in human diseases, Biochim. Biophys. Acta - Mol. Cell Res. 1773 (2007) 1358–1375, 10.1016/j.bbamcr.2007.03.010.

[10]. Schepetkin IA, Kirpotina LN, Hammaker D, Kochetkova I, Khlebnikov AI, Lyakhov SA, Firestein GS, Quinn MT, Anti-inflammatory effects and joint protection in collagen-induced arthritis after treatment with IQ-1S, a selective c-Jun N-terminal kinase inhibitor, J. Pharmacol. Exp. Ther. 353 (2015) 505–516,10.1124/jpet.114.220251. [PubMed: 25784649]

[11]. Atochin DN, Schepetkin IA, Khlebnikov AI, Seledtsov VI, Swanson H, Quinn MT, Huang PL, A novel dual NO-donating oxime and c-Jun N-terminal kinase inhibitor protects against cerebral ischemia-reperfusion injury in mice, Neurosci. Lett. 618 (2016) 45–49, 10.1016/j.neulet.2016.02.033. [PubMed: 26923672]

[12]. Plotnikov MB, Chernysheva GA, Aliev OI, Smol'iakova VI, Fomina TI, Osipenko AN, Rydchenko VS, Anfinogenova YJ, Khlebnikov AI, Schepetkin IA, Atochin DN, Protective Effects of a New C-Jun N-terminal Kinase Inhibitor in the Model of Global Cerebral Ischemia in Rats, Molecules. 24 (2019) 1722 10.3390/molecules24091722.

[13]. Schepetkin IA, Khlebnikov AI, Potapov AS, Kovrizhina AR, Matveevskaya VV, Belyanin ML, Atochin DN, Zanoza SO, Gaidarzhy NM, Lyakhov SA, Kirpotina LN, Quinn MT, Synthesis, biological evaluation, and molecular modeling of 11H-indeno[1,2-b]quinoxalin-11-one derivatives and tryptanthrin-6-oxime as c-Jun N-terminal kinase inhibitors, Eur. J. Med. Chem. 161 (2019) 179–191, 10.1016/j.ejmech.2018.10.023. [PubMed: 30347329]

[14]. Schepetkin IA, Kirpotina LN, Khlebnikov AI, Hanks TS, Kochetkova I, Pascual DW, Jutila MA, Quinn MT, Identification and characterization of a novel class of c-Jun N-terminal kinase inhibitors, Mol. Pharmacol. 81 (2012) 832–845, 10.1124/mol.111.077446. [PubMed: 22434859]

[15]. Giunchedi P, Conti B, Genta I, Conte U, Puglisi G, Emulsion spray-drying for the preparation of albumin-loaded PLGA microspheres, Drug Dev. Ind. Pharm. 27 (2001) 745–750, 10.1081/DDC-100107331. [PubMed: 11694022]

[16]. Ding S, Serra CA, Vandamme TF, Yu W, Anton N, Double emulsions prepared by two-step emulsification: History, state-of-the-art and perspective, J. Control. Release. 295 (2019) 31–49, 10.1016/j.jconrel.2018.12.037. [PubMed: 30579983]

[17]. Cohen-Sela E, Chorny M, Koroukhov N, Danenberg HD, Golomb G, A new double emulsion solvent diffusion technique for encapsulating hydrophilic molecules in PLGA nanoparticles, J. Control. Release. 133 (2009) 90–95, 10.1016/j.jconrel.2008.09.073. [PubMed: 18848962]

[18]. Kudryavtseva VL, Zhao L, Tverdokhlebov SI, Sukhorukov GB, Fabrication of PLA/CaC03 hybrid micro-particles as carriers for water-soluble bioactive molecules, Colloids Surfaces B Biointerfaces. 157 (2017) 481–489, 10.1016/j.colsurfb.2017.06.011. [PubMed: 28654885]

[19]. Jain RA, The manufacturing techniques of various drug loaded biodegradable poly (lactide-co-glycolide) (PLGA) devices, Biomaterials 21 (2000) 2475–2490,10.1016/S0142-9612(00)00115-0. [PubMed: 11055295]

[20]. Prabhakaran MP, Zamani M, Felice B, Ramakrishna S, Electrospraying technique for the fabrication of metronidazole contained PLGA particles and their release profile, Mater. Sci. Eng. C. 56 (2015) 66–73, 10.1016/j.msec.2015.06.018.

[21]. Almería B, Gomez A, Electrospray synthesis of monodisperse polymer particles in a broad (60nm-2μm) diameter range: guiding principles and formulation recipes, J. Colloid Interface Sci. 417 (2014) 121–130, 10.1016/j.jcis.2013.11.037. [PubMed: 24407667]

[22]. Valo H, Peltonen L, Vehviläinen S, Karjalainen M, Kostiainen R, Laaksonen T, Hirvonen J, Electrospray encapsulation of hydrophilic and hydrophobic drugs in poly(L-lactic acid) nanoparticles, Small. 5 (2009) 1791–1798, 10.1002/smll.200801907. [PubMed: 19360725]

[23]. Sridhar R, Ramakrishna S, Electrosprayed nanoparticles for drug delivery and pharmaceutical applications, Biomatter. 3 (2013) e24281, 10.4161/biom.24281. [PubMed: 23512013]

[24]. Mir M, Ahmed N, ur Rehman A, Recent applications of PLGA based nanostructures in drug delivery, Colloids Surfaces B Biointerfaces. 159 (2017) 217–231, 10.1016/j.colsurfb.2017.07.038. [PubMed: 28797972]

[25]. Mundargi RC, Babu VR, Rangaswamy V, Patel P, Aminabhavi TM, Nano/micro technologies for delivering macromolecular therapeutics using poly(dl-lactide-co-glycolide) and its derivatives, J. Control. Release. 125 (2008) 193–209, 10.1016/j.jconrel.2007.09.013. [PubMed: 18083265]

[26]. Avgoustakis K, Polylactic-Co-Glycolic Acid (PLGA), Encycl. Biomater. Biomed. Eng. Second Ed. - Four Vol. Set. (2008) 2259–2269. 10.1201/b18990-216.

[27]. ASTM F1877-16, Standard Practice for Characterization of Particles, ASTM International, West Conshohocken, PA, 2016 10.1520/F1877-16.

[28]. Mathematical models of drug release, in: Strateg. to Modify Drug Release from Pharm. Syst, Elsevier, 2015, pp. 63–86. 10.1016/B978-0-08-100092-2.00005-9.

[29]. Hess U, Shahabi S, Treccani L, Streckbein P, Heiss C, Rezwan K, Co-delivery of cisplatin and doxorubicin from calcium phosphate beads/matrix scaffolds for osteosarcoma therapy, Mater. Sci. Eng. C. 77 (2017) 427–435, 10.1016/j.msec.2017.03.164.

[30]. Schepetkin IA, Kirpotina LN, Khlebnikov AI, Quinn MT, High-throughput screening for small-molecule activators of neutrophils: identification of novel N-formyl peptide receptor agonists, Mol. Pharmacol. 71 (2007) 1061–1074,10.1124/mol.106.033100. [PubMed: 17229869]

[31]. Aftab S, Shah A, Nadhman A, Kurbanoglu S, Aysil Ozkan S, Dionysiou DD, Shukla s.s, Aminabhavi TM, Nanomedicine: An effective tool in cancer therapy, Int. J. Pharm. 540 (2018) 132–149, 10.1016/j.ijpharm.2018.02.007. [PubMed: 29427746]

[32]. Deshmukh AS, Chauhan PN, Noolvi MN, Chaturvedi K, Ganguly K, Shukla SS, Nadagouda MN, Aminabhavi TM, Polymeric micelles: Basic research to clinical practice, Int. J. Pharm. 532 (2017) 249–268, 10.1016/j.ijpharm.2017.09.005. [PubMed: 28882486]

[33]. Poncelet D, Neufeld RJ, Goosen MFA, Burgarski B, Babak V, Formation of microgel beads by electric dispersion of polymer solutions, AIChE J. 45 (1999) 2018–2023, 10.1002/aic.690450918.

[34]. Bock N, Woodruff MA, Hutmacher DW, Dargaville TR, Electrospraying, a reproducible method for production of polymeric microspheres for biomedical applications, Polymers (Basel). 3 (2011) 131–149, 10.3390/polym.3010131.

[35]. Jaworek A, Electrospray droplet sources for thin film deposition, J. Mater. Sci. 42 (2007) 266–297, 10.1007/s10853-006-0842-9.

[36]. Han FY, Thurecht KJ, Whittaker AK, Smith MT, Bioerodable PLGA-based microparticles for producing sustained-release drug formulations and strategies for improving drug loading, Front. Pharmacol. 7 (2016), 10.3389/fphar.2016.00185.

[37]. Xie J, Lim LK, Phua Y, Hua J, Wang C-H, Electrohydrodynamic atomization for biodegradable polymeric particle production, J. Colloid Interface Sci. 302 (2006) 103–112, 10.1016/j.jcis.2006.06.037. [PubMed: 16842810]

[38]. Enayati M, Chang MW, Bragman F, Edirisinghe M, Stride E, Electrohydrodynamic preparation of particles, capsules and bubbles for biomedical engineering applications, Colloids Surfaces A Physicochem. Eng. Asp. 382 (2011) 154–164, 10.1016/j.colsurfa.2010.11.038.

[39]. Ghayempour S, Mortazavi SM, Fabrication of micro-nanocapsules by a new electrospraying method using coaxial jets and examination of effective parameters on their production, J. Electrostat. 71 (2013) 717–727, 10.1016/j.elstat.2013.04.001.

[40]. Xu Y, Skotak M, Hanna M, Electrospray encapsulation of water-soluble protein with polylactide. I. Effects of formulations and process on morphology and particle size, J. Microencapsul. 23 (2006) 69–78, 10.1080/02652040500435048. [PubMed: 16830978]

[41]. Gasmi H, Siepmann F, Hamoudi MC, Danede F, Verin J, Willart J-F, Siepmann J, Towards a better understanding of the different release phases from PLGA microparticles: Dexamethasone-loaded systems, Int. J. Pharm. 514 (2016) 189–199, 10.1016/j.ijpharm.2016.08.032. [PubMed: 27543353]

[42]. Nie H, Lee LY, Tong H, Wang C-H, PLGA/chitosan composites from a combination of spray drying and supercritical fluid foaming techniques: New carriers for DNA delivery, J. Control. Release. 129 (2008) 207–214, 10.1016/j.jconrel.2008.04.018. [PubMed: 18539352]

[43]. da Silva-Junior AA, de Matos JR, Formariz TP, Rossanezi G, Scarpa MV, do Egito EST, de Oliveira AG, Thermal behavior and stability of biodegradable spray-dried microparticles containing triamcinolone, Int. J. Pharm. 368 (2009) 45–55, 10.1016/j.ijpharm.2008.09.054. [PubMed: 18992313]

[44]. Nath SD, Son S, Sadiasa A, Min YK, Lee BT, Preparation and characterization of PLGA microspheres by the electrospraying method for delivering simvastatin for bone regeneration, Int. J. Pharm. 443 (2013) 87–94, 10.1016/j-ijpharm.2012.12.037. [PubMed: 23291448]

[45]. Hyvönen S, Peltonen L, Karjalainen M, Hirvonen J, Effect of nanoprecipitation on the physicochemical properties of low molecular weight poly(l-lactic acid) nanoparticles loaded with salbutamol sulphate and beclomethasone dipropionate, Int. J. Pharm. 295 (2005) 269–281, 10.1016/j.ijpharm.2005.02.026. [PubMed: 15848011]

[46]. Zhang H, Gao S, Temozolomide/PLGA microparticles and antitumor activity against Glioma C6 cancer cells in vitro, Int. J. Pharm. 329 (2007) 122–128,10.1016/j.ijpharm.2006.08.027. [PubMed: 17000068]

[47]. Differential Scanning Calorimetry and Thermogravimetric Analysis, in: Solid State Prop. Pharm. Mater., John Wiley & Sons, Inc, Hoboken, 2017, pp. 124–141. 10.1002/9781119264408.ch10.

[48]. Tseng C-H, Chen Y-LY-R, Tzeng C-C, Liu W, Chou C-K, Chiu C-C, Chen Y-LY-R, Discovery of indeno[1,2-b]quinoxaline derivatives as potential anticancer agents, Eur. J. Med. Chem. 108 (2016) 258–273, 10.1016/j.ejmech.2015.11.031. [PubMed: 26686931]

[49]. Silva-Júmior AA, Scarpa MV, Pestana KC, Mercuri LP, de Matos JR, de Oliveira AG, Thermal analysis of biodegradable microparticles containing ciprofloxacin hydrochloride obtained by spray drying technique, Thermochim. Acta. 467 (2008) 91–98, 10.1016/j.tca.2007.10.018.

[50]. Mainardes RM, Gremião MPD, Evangelista RC, Thermoanalytical study of praziquantel-loaded PLGA nanoparticles, Rev. Bras. Ciências Farm. 42 (2006) 523–530, 10.1590/S1516-93322006000400007.

[51]. Ding L, Lee T, Wang C-H, Fabrication of monodispersed Taxol-loaded particles using electrohydrodynamic atomization, J. Control. Release. 102 (2005) 395–413, 10.1016/j.jconrel.2004.10.011. [PubMed: 15653160]

[52]. Jeon H-J, Jeong Y-I, Jang M-K, Park Y-H, Nah J-W, Effect of solvent on the preparation of surfactant-free poly(dl-lactide-co-glycolide) nanoparticles and norfloxacin release characteristics, Int. J. Pharm. 207 (2000) 99–108, 10.1016/S0378-5173(00)00537-8. [PubMed: 11036235]

[53]. Kumari A, Yadav SK, Yadav SC, Biodegradable polymeric nanoparticles based drug delivery systems, Colloids Surfaces B Biointerfaces. 75 (2010) 1–18,10.1016/j.colsurfb.2009.09.001. [PubMed: 19782542]

[54]. Hosseini SF, Zandi M, Rezaei M, Farahmandghavi F, Two-step method for encapsulation of oregano essential oil in chitosan nanoparticles: Preparation, characterization and in vitro release study, Carbohydr. Polym. 95 (2013) 50–56, 10.1016/j.carbpol.2013.02.031. [PubMed: 23618238]

[55]. Soppimath KS, Aminabhavi TM, Kulkarni AR, Rudzinski WE, Biodegradable polymeric nanoparticles as drug delivery devices, J. Control. Release. 70 (2001) 1–20, 10.1016/S0168-3659(00)00339-4. [PubMed: 11166403]

[56]. Kamaly N, Yameen B, Wu J, Farokhzad OC, Degradable controlled-release polymers and polymeric nanoparticles: mechanisms of controlling drug release, Chem. Rev. 116 (2016) 2602–2663, 10.1021/acs.chemrev.5b00346. [PubMed: 26854975]

[57]. Siepmann J, Modeling of drug release from delivery systems based on hydroxypropyl methylcellulose (HPMC), Adv. Drug Deliv. Rev. 48 (2001) 139–157, 10.1016/S0169-409X(01)00112-0. [PubMed: 11369079]

[58]. Fox S, Leitch AE, Dufifin R, Haslett C, Rossi AG, Neutrophil apoptosis: relevance to the innate immune response and inflammatory disease, J. Innate Immun. 2 (2010) 216–227, 10.1159/000284367. [PubMed: 20375550]

[59]. Cecchi I, Arias de la Rosa I, Menegatti E, Roccatello D, Collantes-Estevez E,Lopez-Pedrera C, Barbarroja N, Neutrophils: Novel key players in Rheumatoid Arthritis. Current and future therapeutic targets, Autoimmun. Rev. 17 (2018) 1138–1149, 10.1016/j.autrev.2018.06.006. [PubMed: 30217550]

[60]. O'Neil LJ, Kaplan MJ, Neutrophils in rheumatoid arthritis: breaking immune tolerance and fueling disease, Trends Mol. Med. 25 (2019) 215–227, 10.1016/j.molmed.2018.12.008. [PubMed: 30709614]

[61]. Tanaka D, Kagari T, Doi H, Shimozato T, Essential role of neutrophils in anti-type II collagen antibody and lipopolysaccharide-induced arthritis, Immunology 119 (2006) 195–202, 10.1111/j.1365-2567.2006.02424.x. [PubMed: 16836650]

[62]. Bisso PW, Gaglione S, Guimaraes PPG, Mitchell MJ, Langer R, Nanomaterial interactions with human neutrophils, ACS Biomater. Sci. Eng. 4 (2018) 4255–4265, 10.1021/acsbiomaterials.8b01062. [PubMed: 31497639]

[63]. Rudt S, Müller RH, In vitro phagocytosis assay of nano- and microparticles by chemiluminescence. I. Effect of analytical parameters, particle size and particle concentration, J. Control. Release. 22 (1992) 263–271, 10.1016/0168-3659(92)90101-V.

[64]. Stankevich KS, Schepetkin IA, Goreninskii SI, Lavrinenko AK, Bolbasov EN, Kovrizhina AR, Kirpotina LN, Filimonov VD, Khlebnikov AI, Tverdokhlebov SI, Quinn MT, Poly(s-caprolactone) Scaffolds doped with c-Jun N-terminal kinase inhibitors modulate phagocyte activation, ACS Biomater. Sci. Eng. 5 (2019) 5990–5999, 10.1021/acsbiomaterials.9b01401.

[65]. Guo Q, Wang Y, Xu D, Nossent J, Pavlos NJ, Xu J, Rheumatoid arthritis: pathological mechanisms and modern pharmacologic therapies, Bone Res. 6 (2018) 15, 10.1038/s41413-018-0016-9. [PubMed: 29736302]

[66]. Arango Duque G, Descoteaux A, Macrophage cytokines: involvement in immunity and infectious diseases, Front. Immunol. 5 (2014), 10.3389/fimmu.2014.00491.

[67]. Kinne RW, Bräuer R, Stuhlmüller B, Palombo-Kinne E, Burmester G-R, Macrophages in rheumatoid arthritis, Arthritis Res. Ther. 2 (2000) 189, 10.1186/ar86.

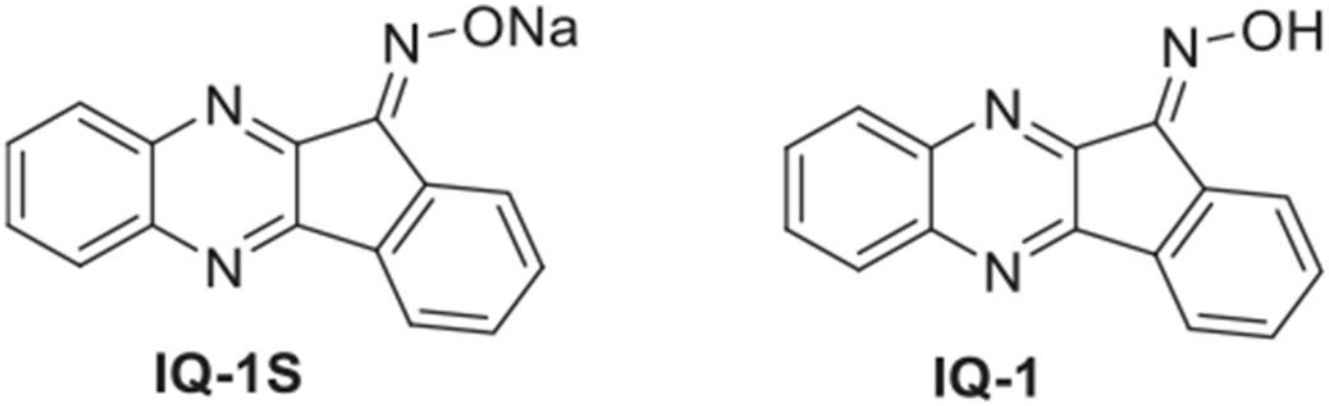

Fig. 1.

Chemical structures of novel c-Jun N-terminal kinase inhibitors: 11*H*-indeno[1,2-*b*]quinoxalin-11-one oxime sodium salt (IQ-1S) and 11*H*-indeno [1,2-*b*]quinoxalin-11-one oxime (IQ-1).

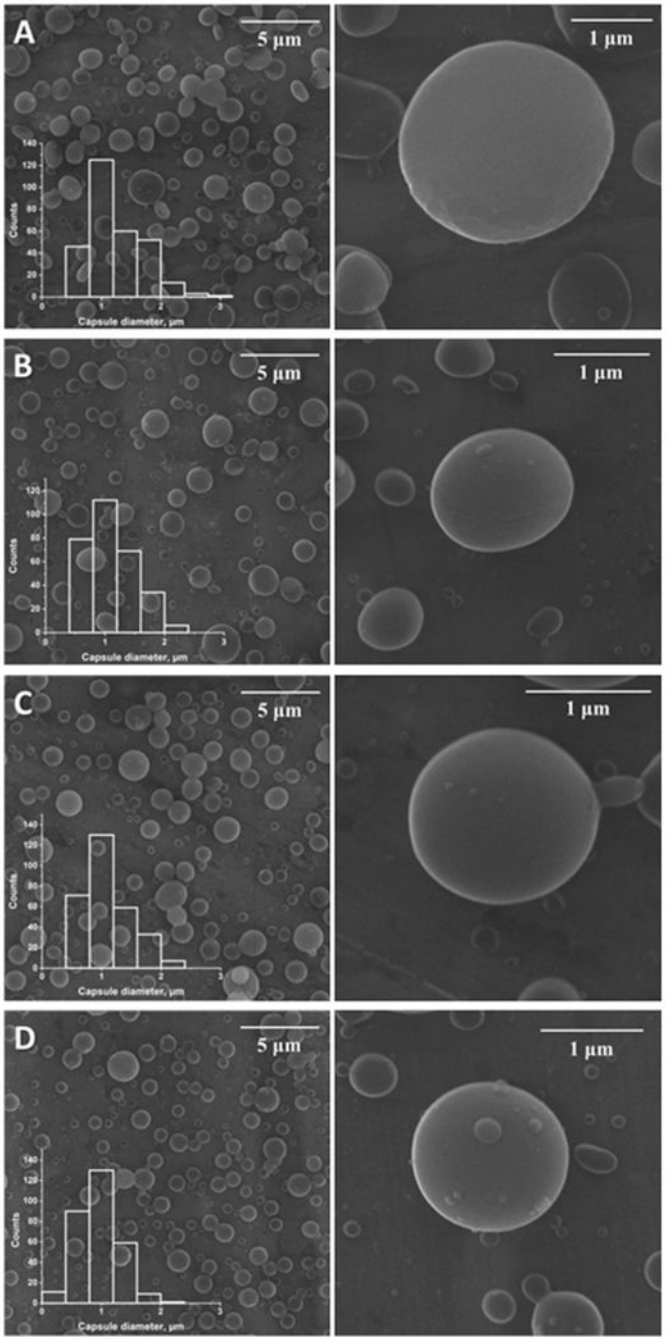

Fig. 2.

Scanning electron microscopy images of the particles and particle diameter distribution. **Panel A:** SEM images of the particles PLGA_0; **Panel B:** SEM images of the particles PLGA_5; **Panel C:** SEM images of the particles PLGA_10; **Panel D:** SEM images of the particles PLGA_20.

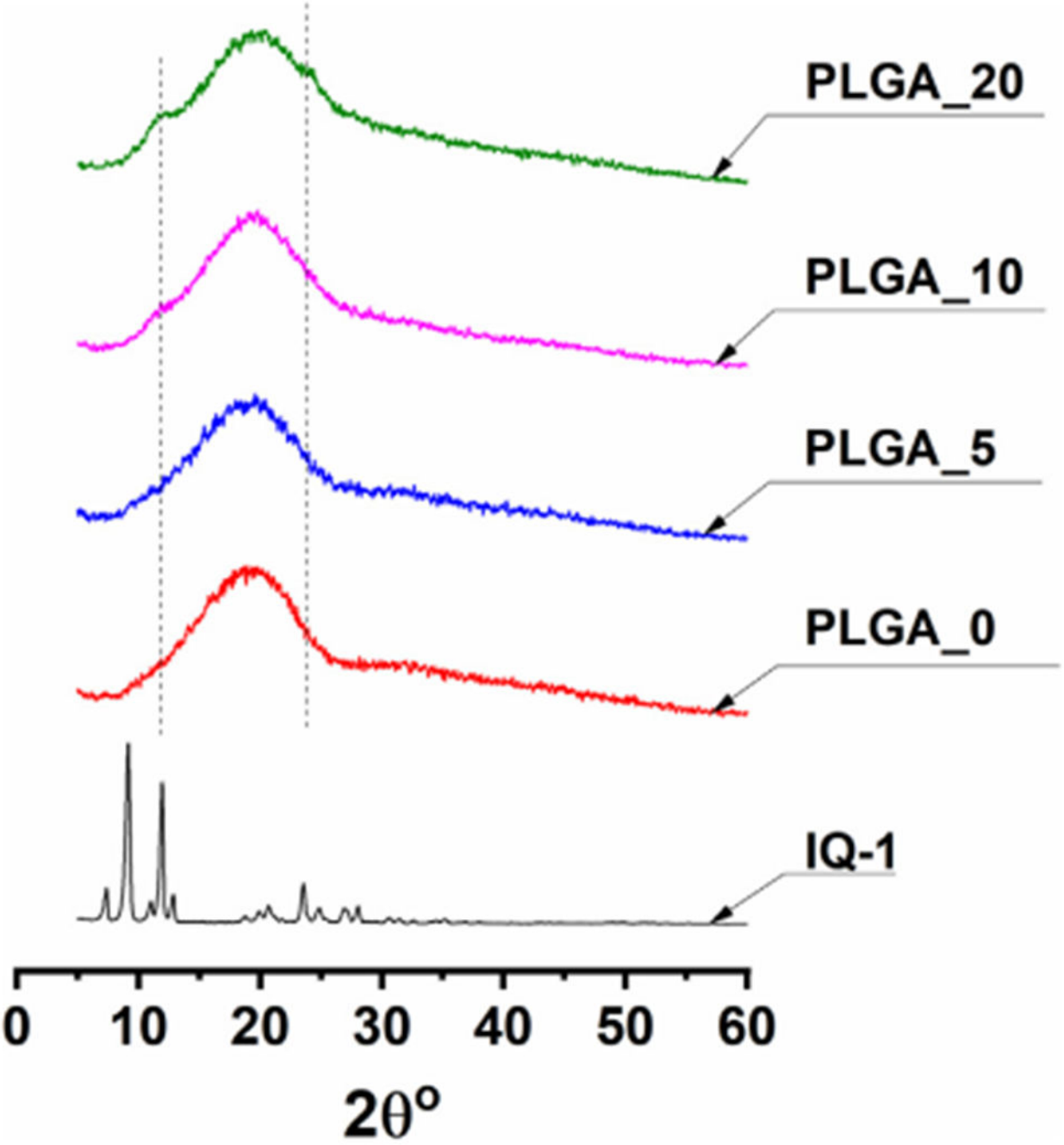

Fig. 3.
XRD results of powdered IQ-1 and PLGA microparticles. Measurements were conducted in the range of angles 2θ 0 – 90°, shooting speed of 2° per min, and step of 0.02°.

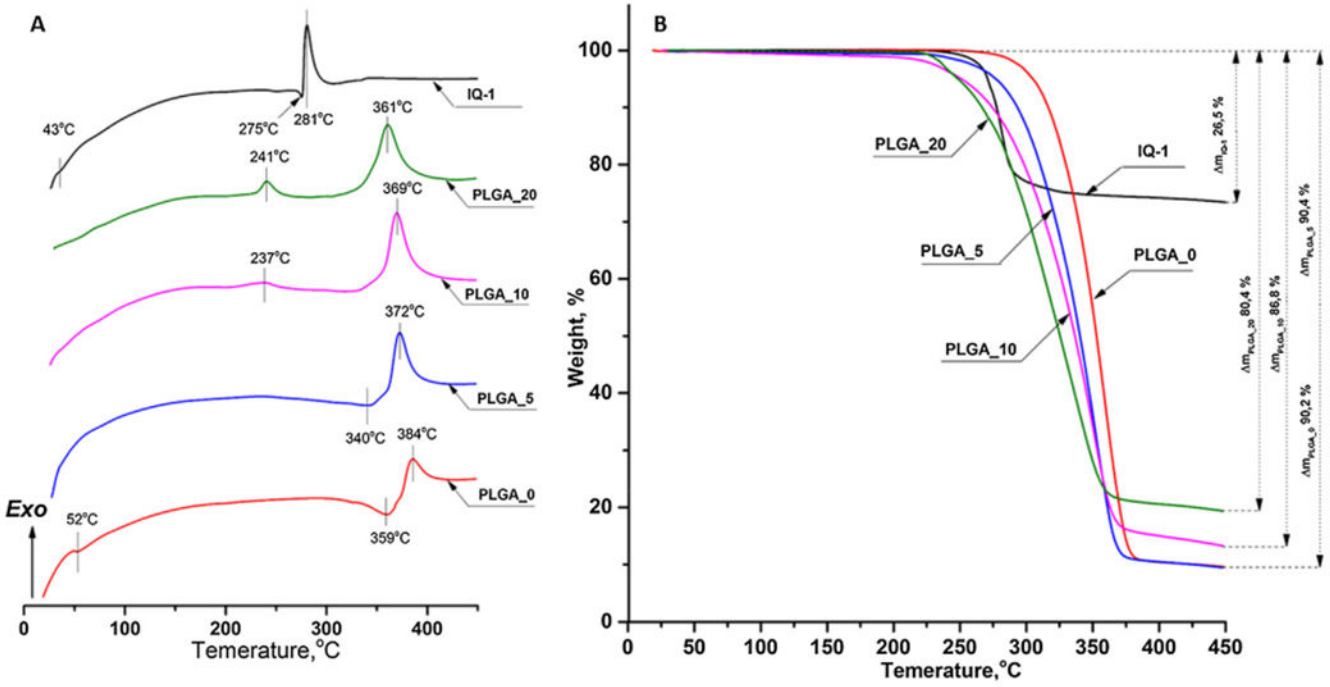

Fig. 4.

Thermal analysis of powdered IQ-1 and PLGA microparticles: **A)** DSC results; **B)** TGA curves. The experiment was performed under dynamic air atmosphere 100 mL per min, heating rate of 10 °C per min, and a temperature range from 25 °C to 450 °C.

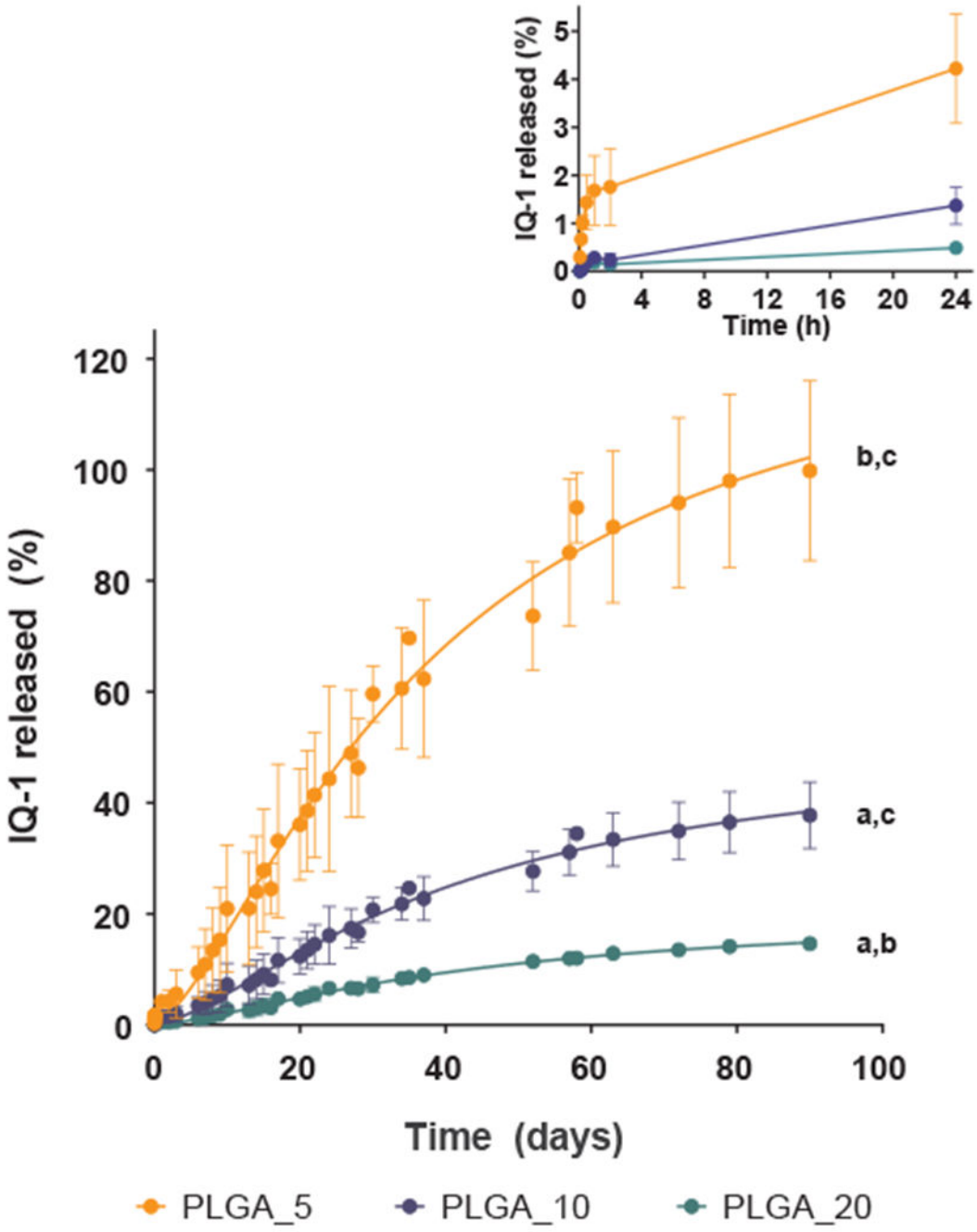

Fig. 5.

Drug release profiles of IQ-1 from PLGA particles. Fabricated particles doped with the IQ-1 were incubated in PBS at 37 °C for 90 days, and the amount of compound released into the medium was determined spectrophotometrically. Non-loaded PLGA particles were used as a reference. The data are presented as mean ± SD of 3 replicates from one experiment, and a representative experiment from three independent experiments is shown. The drug release profiles of PLGA_5, PLGA_10 and PLGA_20 are significantly different from each other (p

< 0.0001 compared to PLGA_5 (a), to PLGA_10 (b), and to PLGA_20 (c); one-way ANOVA with Tukey's correction).

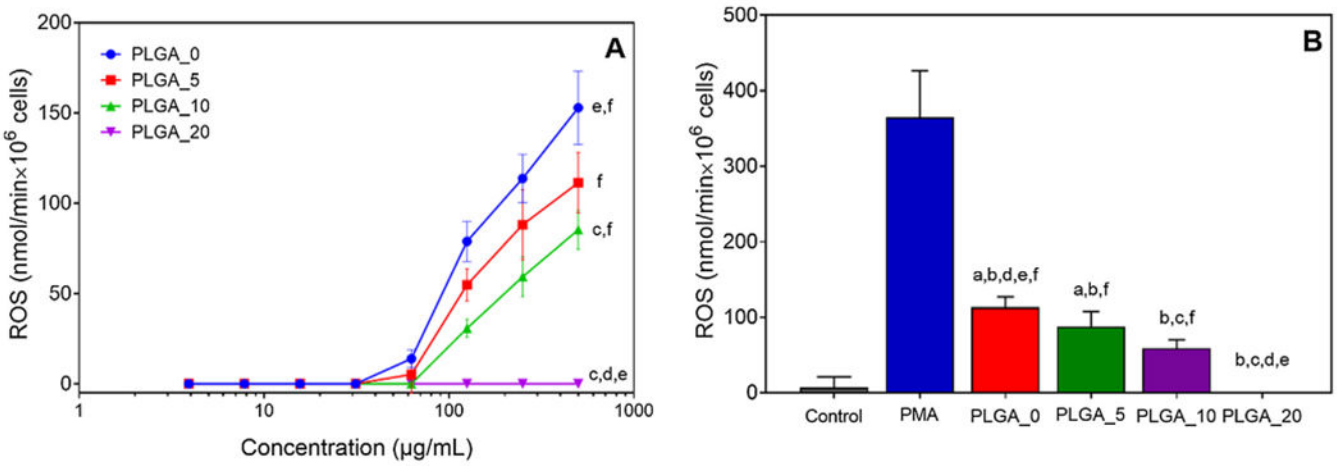

Fig. 6.

Effects of PLGA_0 and PLGA/IQ-1 particles on ROS production by human neutrophils: **A)** dose response study; **B)** ROS production in response to particles added at 250 μg/mL. ROS production was monitored over 2 h using the cytochrome *C* reduction assay. The amount of cytochrome *C* reduced over 2 h is shown. Neutrophils incubated without particles were used as negative control. Neutrophils incubated without particles and stimulated with 100 nM PMA were used as positive control. The data are presented as mean ± SD of 2 replicates from one experiment, and a representative experiment from three independent experiments is shown. Significant differences compared to the medium negative control (a), PMA positive control (b), PLGA_0 (c), PLGA_5 (d), PLGA_10 (e), and PLGA_20 (f) are indicated ($p < 0.0001$; one-way ANOVA with Tukey's correction).

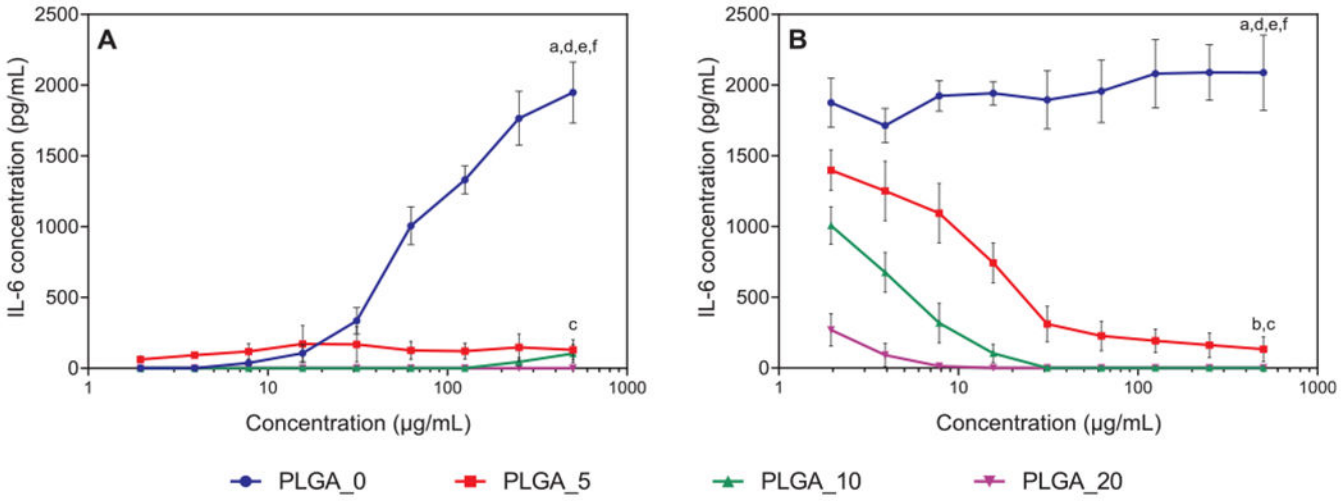

Fig. 7.

Effects of PLGA_0 and PLGA/IQ-1 particles on IL-6 secretion by MonoMac-6 cells: A) PLGA_0 and PLGA/IQ-1 particles incubated with particles for 24 h without stimulation; B) PLGA_0 and PLGA/IQ-1 particles were pre-incubated with MonoMac-6 cells for 30 min, followed by the addition of 200 ng/mL LPS. IL-6 secretion was measured by ELISA in the cell supernatants after a 24-h incubation. The data are presented as mean ± SD of 2 replicates from one experiment, and a representative experiment from three independent experiments is shown. Significant differences compared to the medium negative control (a), LPS positive control (b), PLGA_0 (c), PLGA_5 (d), PLGA_10 (e), and PLGA_20 (f) are indicated ($p < 0.0001$; one-way ANOVA with Tukey's correction).

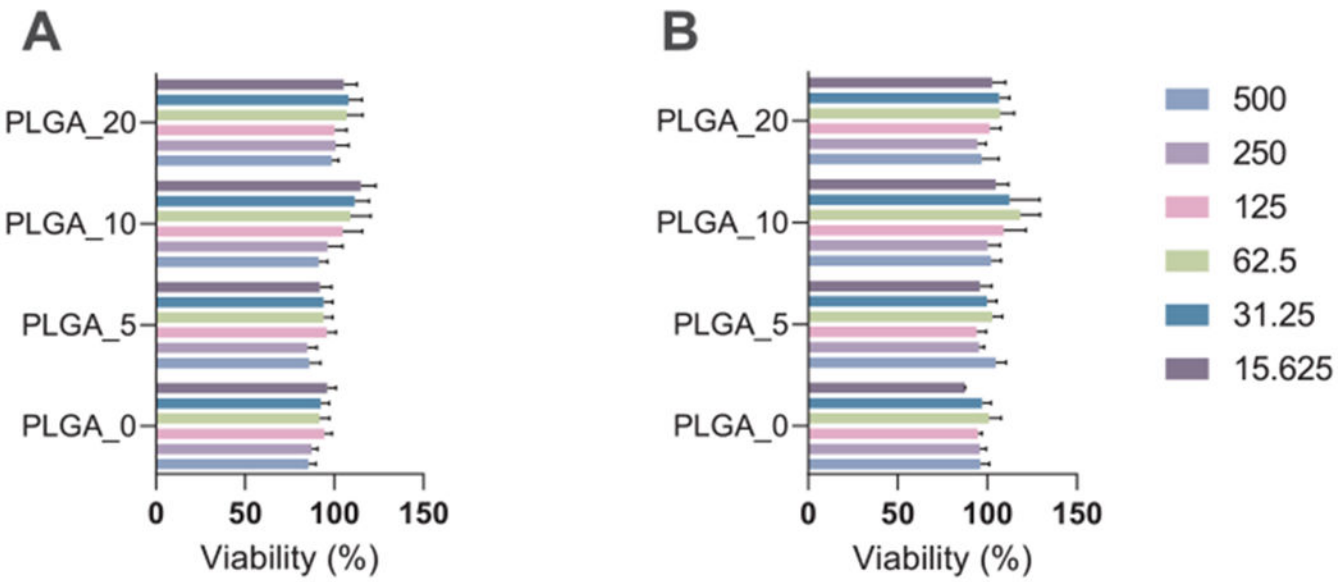

Fig. 8.

The effect of PLGA_0 and PLGA/IQ-1 particles on MonoMac-6 cell viability: A) PLGA_0 and PLGA/IQ-1 particles incubated with particles for 24 h without stimulation; B) PLGA_0 and PLGA/IQ-1 particles were pre-incubated with MonoMac-6 cells for 30 min, followed by the addition of 200 ng/mL LPS. Cell viability was analyzed using a CellTiter-Glo® Luminescent Cell Viability Assay. The data are presented as mean ± SD of 2 replicates from one experiment, and a representative experiment from three independent experiments is shown. The differences between biomaterials are insignificant (one-way ANOVA with Tukey's correction).

Table 1

Microparticle characteristics.

	PLGA_0	PLGA_5	PLGA_10	PLGA_20
Theoretical drug loading, %	0	5	10	20
Practical drug loading, %	-	1.2 ± 0.4	3.8 ± 0.6	12.0 ± 2.8
Encapsulation efficiency, %	-	25 ± 8	40 ± 6	64 ± 13
Particle diameter (d_{max}), μm	1.23 ± 0.45	1.10 ± 0.39	1.10 ± 0.38	0.97 ± 0.33
Aspect ratio	1.17 ± 0.63	1.07 ± 0.56	1.10 ± 0.57	1.04 ± 0.47

Table 2

Regression coefficients values for the kinetic models.

Mathematical model	Zero-order	First-order	Higuchi	Ritger-Peppas
Equation [28]	$f = k_0\, t$	$f = 1 - e^{-k_1 t}$	$f = k_H\, t^{0.5}$	$f = k_p \cdot t^n$
PLGA_5	0.9454	0.8596	0.9463	0.9455 (n = 0.54)
PLGA_10	0.9567	0.9722	0.9423	0.9715 (n = 0.74)
PLGA_20	0.9637	0.9698	0.9422	0.9465 (n = 0.62)